www.ietdl.org

Published in IET Microwaves, Antennas & Propagation
Received on 16th December 2013
Revised on 10th February 2014
Accepted on 12th March 2014
doi: 10.1049/iet-map.2013.0697

ISSN 1751-8725

Synthesis of linear multi-beam arrays through hierarchical almost difference set-based interleaving

Giacomo Oliveri, Federico Viani, Andrea Massa

ELEDIA Research Center, Department of Information Engineering and Computer Science, University of Trento, Via Sommarive 5, 38123 Trento, Italy
E-mail: andrea.massa@ing.unitn.it

Abstract: The study presents an innovative 'almost difference set (ADS)'-based analytical approach for the design of fully interleaved arrays supporting $Q > 2$ independent functions on a shared aperture. Such a hierarchical subarraying methodology allows one to interweave, on the same lattice, $Q = 2^P$ non-overlapped arrangements with beam properties a-priori predictable from the descriptive parameters of the chosen ADSs. A general formulation for the pattern analysis of subarray layouts is derived and successively employed to assess features and potentialities of the multi-level 'ADS' interleaved scheme. A set of representative numerical results, concerned with different apertures, balancing factors and number of interleaved functions, is presented to give some indications on the effectiveness, the efficiency and the reliability of the proposed approach.

1 Introduction and rationale

Modern antenna arrays for satellite [1] and ground communications [2], electronic warfare [3] and remote sensing [4, 5] applications are often required to enable multiple independent functions on a single shared aperture [6–8]. Such a feature is mainly dictated by the growing need to enhance their stealth performance with respect to side-by-side uniform arrangements. To fit this requirement, array architectures interlacing different functionalities (i.e. 'interleaved arrays') [6, 8] have been successfully proposed because of the advantages in terms of flexibility, costs and fabrication complexity of the feeding network as well as the simplicity of the array elements over standard multi-function layouts [9–12].

On the other hand, it cannot be neglected that designing interleaved arrays is a much more complex and challenging task than that of synthesising non-interspread layouts [6, 8]. Indeed, interleaving different functionalities on the same shared physical aperture reduces the number of degrees of freedom of the synthesis process and a degradation of the beam features [e.g. peak sidelobe level (PSL)] usually arises [6, 8]. To counteract such an undesired effect, different design techniques [10, 12] have been proposed over the years including random techniques [13], stochastic optimisation [6, 14] and hybrid approaches [15] (It is worth pointing out that the more recent optimisation techniques such as the artificial bee colony algorithms [16] could be extended to the solution of array interleaving problems (IPs), as well. However, owing to their non-analytical nature, these methods will not be considered in the following.).

In this framework, analytical methodologies have been recently introduced as a powerful and efficient complement to the existing interleaving techniques [8, 17, 18]. More specifically, almost difference sets (ADSs) [17, 19] and their sub-category called difference sets (DSs) [8] have been exploited to analytically synthesise interlaced arrangements with well-controlled sidelobes for electromagnetic [17] as well as ultrasound [18] applications. This has been mainly motivated by the following features of ADSs [8, 17, 18]:

- *PSL predictability:* Thanks to the a-priori knowledge of the autocorrelation function [20], the corresponding arrays exhibit predictable PSLs.
- *Complementarity*: Since any 'ADS' has the same autocorrelation of its complementary sequence [20], except for a known offset, a fully interleaved layout with low sidelobes can be synthesised by just associating the '0s' and '1s' of the 'ADS' sequence at hand to two different functionalities.
- *Efficiency*: Owing to the analytical properties of the ADSs, the design of 'ADS' arrangements is yielded with negligible computational costs also for large and densely populated apertures.

Thanks to such properties, the application of ADSs has been successfully extended to thinned [21–25] and correlator [26] arrangements. Moreover, the hybridisation with global optimisers has been investigated [26, 27], as well.

Unfortunately, present-day fully analytical interleaving methods cannot support more than two functionalities on the same shared aperture because of the 'ADS complementarity' property [8, 17, 18]. However, an analytical synthesis method able to interlace multiple (i.e. more than two) functionalities with predictable radiation

features would be of great interest for the designers of shared aperture arrays [3] especially when dealing with large layouts generally intractable for global optimisation techniques.

Towards this end, this paper is aimed at proposing an innovative design approach that exploits the advantages of analytically based layouts in terms of a-priori known pattern features and efficiency, while interweaving more than two functionalities on the same physical aperture. More specifically, a hierarchical ADS-based methodology able to interleave $Q=2^P$ functions [In this paper, Q identifies the number of (narrowband and isophoric) arrays that share the same aperture.] by subarraying P suitable 'ADS' sequences is introduced.

This paper is organised as follows. Firstly, the IP is stated and the background on existing ADS-based synthesis approaches is summarised (Section 2). Afterwards, the hierarchical ADS-based interleaving methodology is detailed (Section 3) and numerically validated (Section 4). Finally, some conclusions are drawn (Section 5).

2 Problem statement and existing ADS-based synthesis procedures

The problem of fully interleaving Q functions over a single linear aperture can be stated as follows [6]:

Fully IP: Given a lattice of N elements spaced by d wavelengths and Q interleaved functions ($N>Q$), find the membership vector $\underline{\boldsymbol{w}}_q=\{w_q(n)\in\{0,\ 1\};\ n=0,\ \ldots,\ N-1\},\ q=0,\ \ldots,\ Q-1$ that satisfies the following conditions: (*a*) $w_r(n)\times w_s(n)=0,\ n=0,\ \ldots,\ N-1,\ r,\ s\in[0,\ Q-1],\ r\neq s$ and (*b*) $\mathrm{PSL}^{\mathrm{ave}}=\frac{1}{Q}\sum_{q=0}^{Q-1}\mathrm{PSL}\{\boldsymbol{w}_q\}$ ($\mathrm{PSL}^{\mathrm{ave}}$ represents the average PSL of the Q interleaved functions.) is minimum

where the PSL of the qth function, $\mathrm{PSL}\{\boldsymbol{w}_q\}$, is given by [28]

$$\mathrm{PSL}\{\boldsymbol{w}_q\}\triangleq\frac{\max_{|u|>U_q}\left|F_q(u)\right|^2}{\left|F_q(0)\right|^2},\quad q=0,\ \ldots,\ Q-1 \tag{1}$$

Moreover, the normalised array factor is equal to [28]

$$F_q(u)=\frac{\sum_{n=0}^{N-1}w_q(n)\exp(i2\pi n\,\mathrm{d}u)}{K_q},\quad q=0,\ \ldots,\ Q-1 \tag{2}$$

U_q being the mainlobe region (In this paper, U_q extends up to the first null of the pattern [6].), whereas $u=\sin(\theta)$ and $K_q\triangleq\sum_{n=0}^{N-1}w_q(n)$ is the total number of antennas used by the qth function.

In [8, 17, 18], the 'IP' is solved when $Q=2$ (i.e. interleaving of two functions on a shared aperture) by exploiting the complementarity properties of 'ADS' binary sequences. Towards this end, the following theorems have been profitably applied [17].

Theorem 1: If $\boldsymbol{a}$ is an (N, K, Λ, t)-ADS then its complementary sequence $\bar{\boldsymbol{a}}=\{1-a(n),\ n=0,\ \ldots,\ N-1\}$ is an (N, $N-K$, $N-2K+\Lambda$, t)-ADS.

Λ and t being parameters which define the autocorrelation properties of the 'ADS' $\boldsymbol{a}$ [18] (By definition, $\boldsymbol{a}$ is a binary sequence of length N such that $\sum_{n=0}^{N-1}a(n)=K$ and characterised by an autocorrelation function given by $\xi(\tau)\triangleq\sum_{n=0}^{N-1}a(n)a\left[(n+\tau)\right]_{\mathrm{mod}N}\Big]=\{K$ for $\tau=0;\ \Lambda$ for t values of $\tau\in[0,\ N-1];\ \Lambda+1$ else$\}$, where $(\cdot)\rfloor_N$ stands for the reminder of the division by N [20]. Properties and construction techniques of ADSs can be found in [19, 20, 29, 30], whereas examples of ADSs are available in [31].).

Theorem 2: If $\boldsymbol{a}$ is an (N, K, Λ, t)-ADS then the sequence $\left\{a\left[(n+\sigma)\right]_{\mathrm{mod}N}\right\};\ n=0,\ \ldots,\ N-1$ ($\sigma=0,\ \ldots,\ N-1$, σ being the cyclic shift) is an (N, K, Λ, t)-ADS with the same autocorrelation properties.

According to these theorems and thanks to the autocorrelation properties of the 'ADS' [17], the samples of the power patterns of the $Q=2$ interleaved arrays are a-priori computable from the (known) autocorrelation $\xi(\tau)$ and they are given by

$$\begin{cases}\left|F_0\left(\dfrac{k}{\mathrm{d}N}\right)\right|^2=\dfrac{\sum_{\tau=0}^{N-1}\xi(\tau)\exp\left(\frac{2\pi i\tau k}{N}\right)}{K_0^2}\\ \left|F_1\left(\dfrac{k}{\mathrm{d}N}\right)\right|^2=\dfrac{\sum_{\tau=0}^{N-1}\left[\xi(\tau)+N-2K\right]\exp\left(\frac{2\pi i\tau k}{N}\right)}{K_1^2}\\ k\in\mathbb{N}\end{cases} \tag{3}$$

Such a knowledge has been profitably exploited to deduce suitable 'PSL' bounds [22]. Moreover, a computationally efficient synthesis technique has been implemented for the $Q=2$ case [17].

3 Hierarchical interleaving methodology

To fully interleave $Q=2^P$ functionalities on a single aperture still retaining the positive features of the ADSs, an ADS-based hierarchical approach is proposed. In the following sections, the procedure is detailed starting from an analysis of overlapped structures up to the synthesis of binary fully interleaved architectures without shared elements.

3.1 Interleaved arrays through hierarchical architectures

With reference to the more general case of overlapped structures, let us factorise N as the product of $P=\log_2 Q$ integers, $N=\prod_{p=0}^{P-1}N^{(p)}$ and let us introduce a hierarchical subarray architecture [7] where the pth level vector related to the qth function is $\boldsymbol{s}_q^{(p)}=\left\{s_q^{(p)}(n)\in\mathbb{C},\ n=0,\ \ldots,\ N^{(p)}-1\right\}$ (Fig. 1). The 'effective' nth element weight [7] of the qth beam (Fig. 1) turns out to be equal to (see Appendix)

$$w_q(n)=\prod_{p=0}^{P-1}s_q^{(p)}\left[\left(n\div L^{(p-1)}\right)\rfloor_{\mathrm{mod}N^{(p)}}\right],\quad n=0,\ \ldots,\ N-1 \tag{4}$$

where the operation $(x\div y)$ stands for the quotient of x divided by y and

$$L^{(p-1)}\triangleq\begin{cases}1, & \text{if}\quad p=0\\ N^{(0)}\times\cdots\times N^{(p-1)}, & \text{otherwise}\end{cases}$$

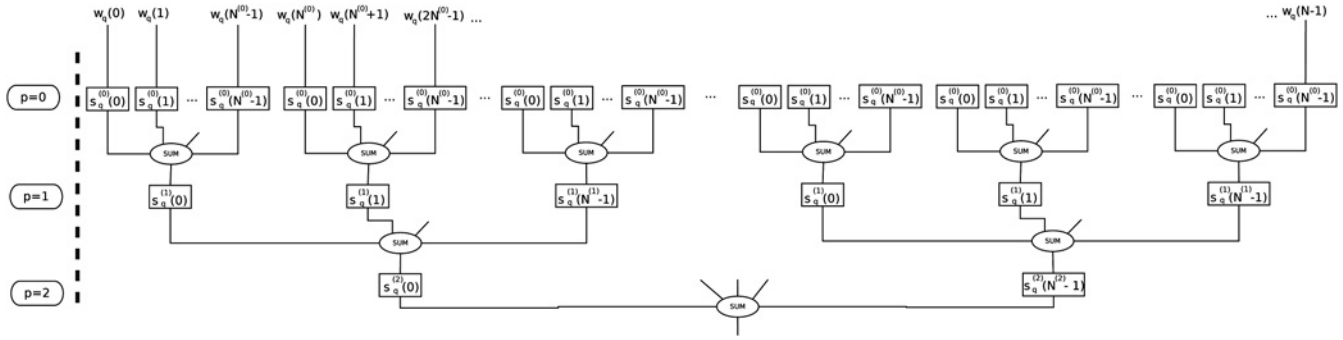

Fig. 1 *Reference array geometry ($Q = 8$) – linear array with P-level weighting ($P = 3$)*

Physically, $w_q(n) \in \mathbb{C}$, $n = 1, \ldots, N$, represent the excitation coefficients applied to the N antennas to synthesize the qth function. By substituting (4) in (2), it results that (see Appendix)

$$F_q(u) = \prod_{p=0}^{P-1} \left[F_q^{(p)}(u) \right] \tag{5}$$

where

$$F_q^{(p)}(u) \triangleq \frac{\sum_{n=q}^{N^{(p)}-1} s_q^{(p)}(n) \exp\left(i2\pi n d^{(p)} u\right)}{K_q^{(p)}}, \quad p = 0, \ldots, P-1 \tag{6}$$

is the contribution of the pth level of the hierarchical architecture to the array factor [7], whereas $K_q^{(p)} \triangleq \left[\sum_{n=0}^{N^{(p)}-1} s_q^{(p)}(n) \right]$ and

$$d^{(p)} \triangleq \begin{cases} d, & \text{if } p = 0 \\ d \times L^{(p-1)}, & \text{otherwise} \end{cases} \tag{7}$$

is the 'effective spacing' between two-adjacent elements of the qth array structure [7]. It is worth noting that (5) is the P-level generalisation of the well-known subarray pattern multiplication formula [7].

3.2 Fully interleaved arrays through hierarchical binary subarraying

Now, let us consider fully interleaved arrays and, for simplicity, the binary case when $s_q^{(p)}(n) \in \{0, 1\}$, $q = 0, \ldots, Q-1$ (i.e. $w_q(n) \in \{0, 1\}$ through (4)). Under this assumption, each function is synthesised by equally weighting a subset of the N available antennas. Pictorially, the 'white' elements in Fig. 2*a* correspond to $s_q^{(p)}(n) = 0$, whereas the 'coloured' ones indicate $s_q^{(p)}(n) = 1$.

Whatever the rule for defining the binary sequence $s_0^{(p)}(n)$, $n = 0, \ldots, N-1$, the membership/beam vector $\boldsymbol{w}_0$ from (4) turns out to be a binary arrangement of $K_0 < N$ 'active' (i.e. connected to the $q = 0$ function feeding point) elements (Fig. 2*b*). The $q = 1$ membership vector, $\boldsymbol{w}_1$, not sharing any element with $\boldsymbol{w}_0$ (i.e. physically non-overlapped), can be then defined by setting the corresponding pth level vector $\boldsymbol{s}_1^{(p)}$ as follows

$$\boldsymbol{s}_1^{(p)} = \begin{cases} \overline{\boldsymbol{s}}_0^{(p)}, & \text{if } p = 0 \\ \boldsymbol{s}_0^{(p)}, & \text{if } p = 1, \ldots, P-1 \end{cases} \tag{8}$$

in order to fulfil the 'fully interleaving' property (*a*) $w_0(n) \times w_1(n) = 0$, $n = 1, \ldots, N$. Therefore the arising array architecture implements two 'non-overlapped' functions by simply switching the $p = 0$ sequence from '0s' (Fig. 2*b*) to '1s' (Fig. 2*c*) and vice-versa [(8)].

To synthesise $Q = 2^P$ perfectly interleaved functions in an N-sized lattice, the previous 'two's complement' procedure can be iterated as follows

$$\boldsymbol{s}_q^{(p)} = \begin{cases} \overline{\boldsymbol{s}}_0^{(p)} & \text{if } \alpha_q^{(p)} = 1 \\ \boldsymbol{s}_0^{(p)} & \text{otherwise} \end{cases}, \quad p = 0, \ldots, P-1, \quad q = 0, \ldots, 2^P - 1 \tag{9}$$

where $\alpha_q = \left\{ \alpha_q^{(p)};\ p = 0, \ldots, P-1 \right\}$ is the binary representation of q such that $\sum_{p=0}^{P-1} \alpha_q^{(p)} 2^p = q$. For example, the functions $q = 2$ and $q = 3$ are implemented as shown in Figs. 2*d* and *e*, respectively.

As expected, the resulting architecture is fully interleaved, that is, each of the N antennas is physically connected to only one of the Q feeding networks synthesising the independent beams (Fig. 2*a*). Indeed, each qth beam is generated by

$$K_q = \prod_{p=0}^{P-1} K_q^{(p)} = N \left[\prod_{p=0}^{P-1} \nu_q^{(p)} \right], \quad q = 0, \ldots, Q-1 \tag{10}$$

active elements ($\nu_q^{(p)} \triangleq \left[\left\{ K_q^{(p)} \right\} / \left\{ N^{(p)} \right\} \right] < 1$ being the 'fill factor' of $\boldsymbol{s}_q^{(p)}$) and (see Appendix)

$$\sum_{q=0}^{Q-1} K_q = N \tag{11}$$

Thanks to the above, the binary 'IP' can be reformulated as follows

Simplified IP (SIP): Given the lattice size $N = \prod_{p=0}^{P} N^{(p)}$ and the number of interleaved functions $Q = 2^P$, find $\boldsymbol{s}_0^{(p)} = \left\{ s_0^{(p)}(n) \in \{0, 1\};\ n = 0, \ldots, N^{(p)} - 1,\ (p = 0, \ldots, P-1) \right.$ such that $\mathrm{PSL}^{\mathrm{ave}} = (1/Q) \sum_{q=0}^{Q-1} \mathrm{PSL}\left\{ \boldsymbol{w}_q \right\}$ is minimum, $\boldsymbol{w}_q (q = 0, \ldots, Q-1)$ being computed by means of (4) and (9). (It is worthwhile to note that the original *IP* has been significantly simplified since now it is only required the computation of P arbitrary binary

doi: 10.1049/iet-map.2013.0697

sequences of length $N^{(p)}$ instead of $Q=2^P$ jointly interleaved arrangements of length $N=\prod_{p=0}^{P-1}N^{(p)}$.)

3.3 Fully interleaved arrays through hierarchical ADSs subarraying

Despite the simplification of the original *IP* when dealing with hierarchical binary architectures (Section 3.2), the solution of the 'SIP' is again not trivial. Indeed, the arising $\mathrm{PSL}^{\mathrm{ave}}$ still depends on the a-priori unknown sidelobes of the P interleaved arrays at hand (i.e. the choice of $\boldsymbol{s}_0^{(p)}$ and its complementary $\bar{\boldsymbol{s}}_0^{(p)}$, $p=0, \ldots, P-1$). However, there exist complementary interleaved arrangements with low and controllable sidelobes, such as those generated through the 'ADS' design procedure highlighted in Section 2 [17]. Then, let us consider a set of $(N^{(p)}, K^{(p)}, \Lambda^{(p)}, t^{(p)})$-ADSs $\boldsymbol{a}^{(p)}(p=0, \ldots, P-1)$ (either constructed [19, 20] or chosen from available databases [31]) and 'analytically' define the sequences $\boldsymbol{s}_0^{(p)}$ as

$$\boldsymbol{s}_0^{(p)}=\boldsymbol{a}^{(p)}, \quad p=0, \ldots, P-1 \tag{12}$$

to yield that each pth level of the 0th function actually corresponds to an 'ADS' thinned array with spacing $d^{(p)}$ [(6)]. Therefore, by (12), (9) and (6) [and analogously to (3)], the samples of $\left|F_q^{(p)}(u)\right|^2$ can be a-priori computed from the (three-level [20]) autocorrelation $\xi^{(p)}(\tau)=\sum_{n=0}^{N^{(p)}-1}a^{(p)}(n)a^{(p)}\left[(n+\tau)\rfloor_{\mathrm{mod}N^{(p)}}\right]$ (see (13))

retaining the pattern predictability features of the *ADS*-based techniques [17]. Since the same holds true if $\boldsymbol{s}_0^{(p)}$ (12) is computed from a cyclically shifted version of $\boldsymbol{a}^{(p)}$ (Theorem 2), the design procedure resumed in Appendix ('ADS design procedure') is deduced.

3.4 Descriptive example

To detail the proposed methodology (Appendix 'ADS design procedure'), let us consider the following illustrative example concerned with a half-wavelength ($d=0.5$) lattice of $N=120$ elements. To synthesize $Q=4$ (i.e. $P=2$) independent beams, let us firstly factorise the lattice dimension (*Step 2*). Let be $N=N^{(0)}\times N^{(1)}=10\times 12$ our choice. Accordingly, suitable 'ADS' sequences with $N^{(0)}=10$ and $N^{(1)}=12$ have to be selected [31]. For example, let us consider the (10, 5, 2, 7) and (12, 6, 2, 3) ADSs: $\boldsymbol{a}^{(0)}\triangleq[1000101101]$ and $\boldsymbol{a}^{(1)}\triangleq[101001000111]$.

By applying (12), the pth ($p=0, 1$) levels of the $q=0$ beam are then computed ['white' elements in Figs. 2*a* – *Step 4*(*a*)] by setting at the initialisation (*Step 3*) the shift indexes to $\sigma^{(p)}=0, p=0, 1$

$$\begin{cases}\boldsymbol{s}_0^{(0)}=1000101101\\ \boldsymbol{s}_0^{(1)}=101001000111\end{cases}$$

The corresponding 'effective' weight vector $\boldsymbol{w}_0$ turns out to be (4) [*Step 4*(*a*)]

$$\boldsymbol{w}_0=\left[s_j=\boldsymbol{s}_0^{(0)};\ j=0,\ \ldots,\ \left(N^{(1)}-1\right)\right].\mathrm{OR}\left[\mathbf{s}_0^{(1)}(n);\ n=0,\ \ldots,\ \left(N^{(1)}-1\right)\right] \tag{14}$$

where $\boldsymbol{s}_0^{(1)}(n)=\left[s_j=s_0^{(1)}(n); j=0,\ \ldots,\ \left(N^{(0)}-1\right)\right]$, $n=0, \ldots, (N^{(1)}-1)$, that is

$$\begin{aligned}&\boldsymbol{w}_0=\\ &[1000101101100010110110001011 01...].\mathrm{OR}. \quad (p=0)\\ &[1111111111000000000011111111 11...]= \quad (p=1)\\ &[1000101101000000000010001011 01...]\end{aligned} \tag{15}$$

As for the subarray sequences for $q=1$, they are obtained by (9) ['white' ($p=1$) and 'red' ($p=0$) elements in Fig. 2*a* – *Step 4*(*a*)]

$$\begin{cases}\boldsymbol{s}_1^{(0)}=\bar{\boldsymbol{s}}_0^{(0)}=0111010010\\ \boldsymbol{s}_1^{(1)}=\boldsymbol{s}_0^{(1)}=101001000111\end{cases}$$

and

$$\begin{aligned}&\boldsymbol{w}_1=\\ &[0111010010011101001001110100 10\ldots].\mathrm{OR}. \quad (p=0)\\ &[1111111111000000000011111111 11\ldots]= \quad (p=1)\\ &[0111010010000000000000111010 010\ldots]\end{aligned} \tag{16}$$

As expected, the beam coefficients $\boldsymbol{w}_0$ and $\boldsymbol{w}_1$ do not share any element [i.e. $\boldsymbol{w}_0(n)\times\boldsymbol{w}_1(n)=0, n=0, \ldots, N-1-(15)$ against (16)].

By applying the same procedure for the remaining beams (i.e. $q=2, 3$), the layout in Fig. 2*a* is synthesised whose $\mathrm{PSL}^{\mathrm{ave}}$ is then computed according to (1) [*Step 4*(*b*)]. Towards this end, (6) is used to evaluate each ($P=3$)th contribution to the qth array factor, $F_q^{(p)}(u)$, $p=0, 1$, $q=0, \ldots, 3$ (Figs. 3*a* and *b*). These latter are combined according to (5) to obtain the qth array factor $F_q(u)$, $q=0, \ldots, 3$

$$\left|F_q^{(p)}\left(\frac{k}{d^{(p)}N^{(p)}}\right)\right|^2=\begin{cases}\dfrac{\sum_{n=0}^{N^{(p)}-1}\xi^{(p)}(\tau)\exp\left(\dfrac{2\pi i\tau k}{N^{(p)}}\right)}{\left(K_0^{(p)}\right)^2}, & \text{if } \alpha_q^{(p)}=1\\ \dfrac{\sum_{n=0}^{N^{(p)}-1}\left[\xi^{(p)}(\tau)+N^{(p)}-2K_0^{(p)}\right]\exp\left(\dfrac{2\pi i\tau k}{N^{(p)}}\right)}{\left(N^{(p)}-K_0^{(p)}\right)^2}, & \text{otherwise } k\in\mathbb{N}\end{cases} \tag{13}$$

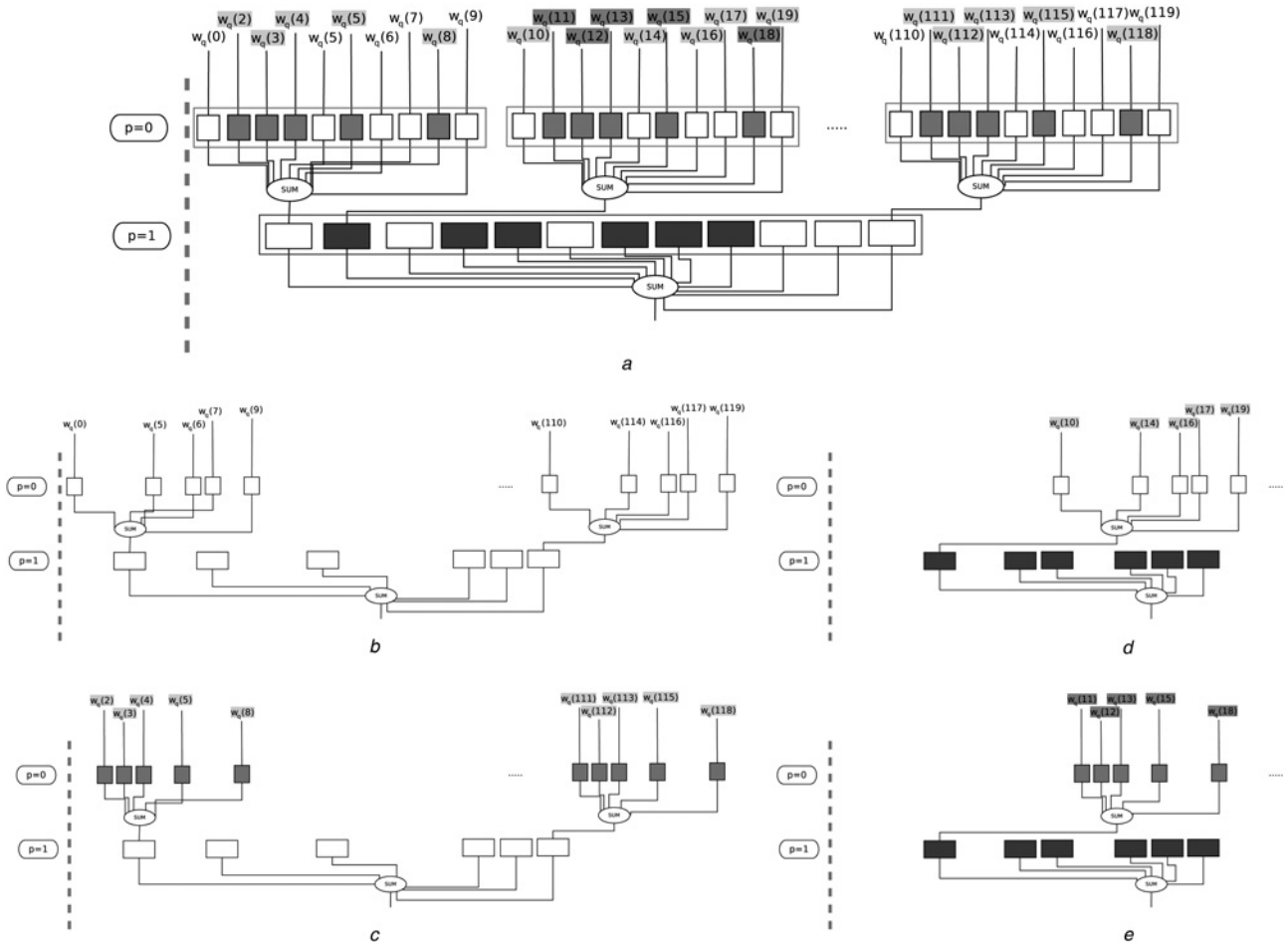

Fig. 2 *Descriptive example ($Q = 4$, $P = 2$, $N = 120$, $N^{(0)} = 10$, $N^{(P-1)} = 12$)*

a Sketch of the subarray weighting of the interleaved arrangement of the qth feeding network
b $q = 0$
c $q = 1$
d $q = 2$
e $q = Q - 1$

(Fig. 3*c*). Such a loop [*Step 4*(*c*)] is then iterated to minimise the $\mathrm{PSL}^{\mathrm{ave}}$ by considering different cyclic shifts until $\sigma^{(p)} = N^{(p)} - 1$, $p = 0, 1$.

As it can be noted, the effective weights computation (4) is a 'copy' and 'multiply' procedure of the basic $\boldsymbol{s}_q^{(p)}$ sequences depending on the level index p [e.g. (14)–(16)]. Thanks to the analytic nature of the method, the whole synthesis requires up to N loops (*Step 4*) each one composed by $\log_2 Q$ binary sequence shifts and $Q \log_2 Q$ binary sequence multiplications [*Step 4*(*a*)]. Owing to (13), $F_q^{(p)}(u)$ presents predictable samples (dots – Figs. 3*a* and *b*) that, after combination, result in known pattern samples of the qth array factor $F_q(u)$ (crosses – Fig. 3*c*). These latter actually corresponds to the highest sidelobes of each qth beam (Fig. 3*c*). Analogously to [17], such samples coincide whatever q if balanced layouts are at hand ($\nu_q^{(p)} = 0.5$, $q = 0, \ldots, Q - 1$, $p = 0, \ldots, P - 1$), as in this descriptive example.

Additionally, it is worth pointing out that no grating lobes appear in $F_q(u)$ ($q = 0, \ldots, 3$) (Fig. 3*c*) despite the average spacing

$$d_q \triangleq \frac{d \times (N-1)}{K_q - 1}$$

is significantly above $\lambda/2$ ($d_q = 2$ for $q = 0, \ldots, 3$) (Fig. 2*c*). Such a feature is actually expected from the 'ADS' theory. As a matter of fact, one can deduce from (5) that

$$F_q(u) = 1 \Leftrightarrow F_q^{(p)}(u) = 1 \quad \forall p = 0, \ \ldots, \ P-1$$

which means that a grating lobe appears at u only if all $F_q^{(p)}(u)$ exhibit a grating lobe along that direction. Since, $F_q^{(0)}(u)$ represents the array factor of an $N^{(0)}$-sized 'ADS' layout with inter-element distance $d^{(0)}$ [(6)], it turns out that grating lobes can be avoided if $d^{(0)} \leq 0.5$ [22] whatever the steering angle. Thus

$$d^{(0)} \leq 0.5 \tag{17}$$

is a sufficient condition to a-priori avoiding grating lobes whatever the value of Q. Such a result is not negligible since only binary (i.e. non-tapered) weights are considered.

Moreover, as concerns the directivity ($D\{\boldsymbol{w}_q\}$) of the Q beams, it is worth noting that such a parameter does not vary with q ($D\{\boldsymbol{w}_q\} \simeq 14.7$ dB – Table 1), because of the balanced nature of the final architecture ($K_q = 30$, $q = 0, \ldots, 3$).

doi: 10.1049/iet-map.2013.0697

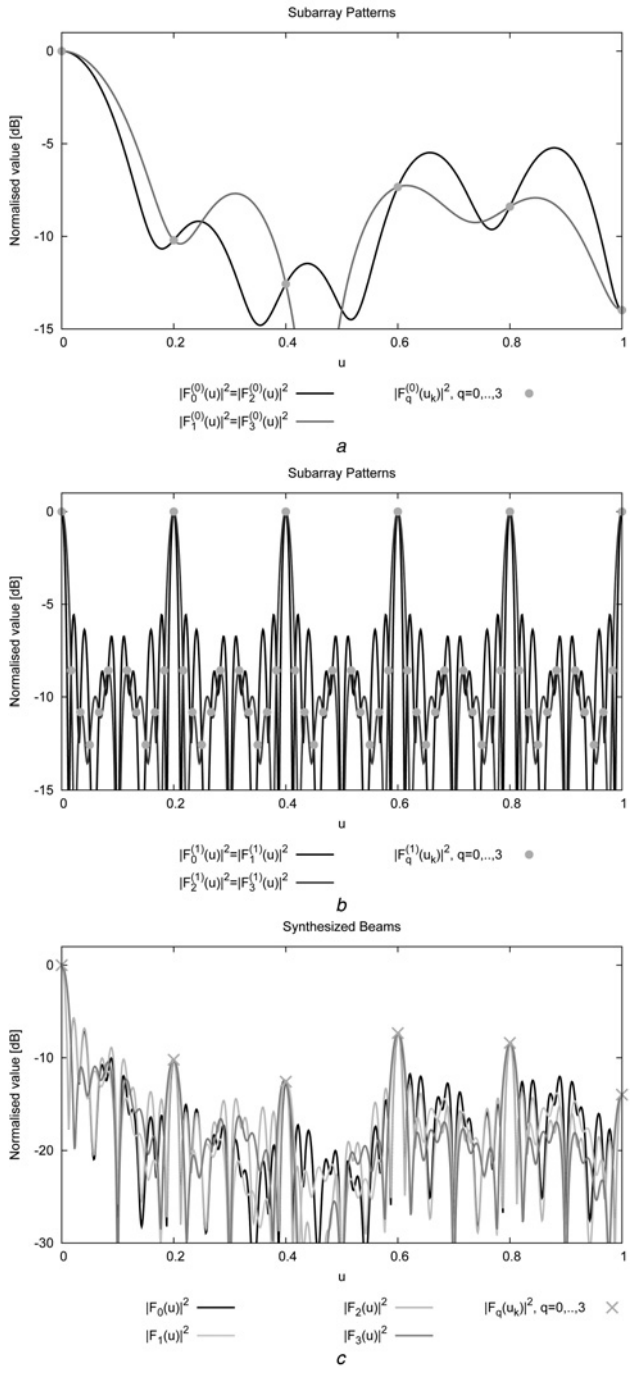

Fig. 3 *Descriptive example ($Q = 4$, $P = 2$, $N = 120$, $N^{(0)} = 10$, $N^{(P-1)} = 12$) – plot of*
a $F_q^{(p)}(u)\big|_{p=0}$
b $F_q^{(p)}(u)\big|_{p=1}$
c $F_q(u)$, along with the predictable pattern samples

On the contrary, the 3 dB beamwidth ($BW\{\boldsymbol{w}_q\}$) depends on the considered function (i.e. $BW\{\boldsymbol{w}_q\} \in [0.69,\ 1.20]°$ – Table 1). As a matter of fact, each function actually employs a different portion of the overall shared region (see Fig. 2), and accordingly the interleaved arrays have (slightly) different widths (e.g. Fig. 2*c* against *e*). However, all the beamwidths are approximately similar to that of the corresponding N-size uniformly illuminated filled array (i.e. $BW^{\text{unif}} \simeq 0.85°$ [28]). Furthermore, such BW differences reduce if wider arrangements are at hand (see Section 4).

Table 1 Descriptive example ($Q = 4$, $P = 2$, $N = 120$, $N^{(0)} = 10$, $N^{(P-1)} = 12$) – Figures of merit of the beams in Fig. 3*c*

q	PSL$\{\boldsymbol{w}_q\}$, dB	$D\{\boldsymbol{w}_q\}$, dB	$BW\{\boldsymbol{w}_q\}$, deg
0	– 5.76	14.7	0.69
1	– 7.29	14.7	1.20
2	– 5.69	14.7	0.69
2	– 7.33	14.7	1.20

4 Numerical assessment and performance analysis

This section is aimed at assessing the effectiveness, the flexibility and the computational efficiency of the proposed 'ADS' approach for 'IPs' with $Q > 2$. Towards this end, a set of representative numerical examples concerned with different aperture sizes ($N \in [100,\ 10\,000]$) (Apertures comprising up to several thousand elements have been considered because of their importance in emerging high-frequency applications such as wireless power transmission [32].), Q values and balancing factors will be presented by showing, besides the arising radiation patterns, the values of the associated figures of merit (i.e. PSL^{opt}, $D^{\text{opt}} \triangleq \frac{1}{Q}\sum_{q=0}^{Q-1} D\left\{\boldsymbol{w}_q\right\}$ and $BW^{opt} \triangleq \frac{1}{Q}\sum_{q=0}^{Q-1} BW\left\{\boldsymbol{w}_q\right\}$ when $\boldsymbol{\sigma}^{(p)} = \boldsymbol{\sigma}_{\text{opt}}^{(p)}$, $p = 0, \ldots, P-1$). Architectures complying with (17) will be synthesised by means of 'ADS' sequences listed in [31].

4.1 Shared aperture arrays with $Q = 4$ interleaved functions

The first set of numerical examples deals with a $N = 100$ balanced layout ($v_q^{(p)} = 0.5$, $q = 0, \ldots, Q-1$, $p = 0, \ldots, P-1$) which has been synthesised by choosing $N^{(0)} = N^{(1)} = 10$ and defining $\boldsymbol{a}^{(p)}$ ($p = 0,\ 1$) as the (10, 5, 2, 7)-ADS [31]. To illustrate the outcomes of 'ADS' design procedure, Fig. 4*a* shows the behaviour of the average PSL computed during the synthesis loop, whereas the final (optimal) patterns are reported in Fig. 4*c*. As it can be noted, the plot of PSL^{ave} against the solution index $N^{(1)}\sigma^{(0)} + \sigma^{(1)}$ (Fig. 4*a*) shows that the grating lobes (i.e. PSL = 0 dB) are avoided [$-7.2 \le \text{PSL}^{\text{ave}} \le -5$ dB – Fig. 4*a*] thanks to (17) whatever the cyclic shift, $\sigma^{(p)} = 0, \ldots, N^{(p)} - 1$ ($p = 0,\ 1$), despite the small arrangement ($K_q = 25$, $q = 0, \ldots, Q-1 = 3$) and the large average spacing ($d_q = 2$) of the interleaved architectures. As expected, all the synthesised beams comply with (13) (Fig. 4*c*), thus confirming the capability of the ADS-based approach to control/predict the pattern lobes of the synthesised layouts. As for the computational issues, the 'central processing unit' time is negligible (e.g. $\Delta t \simeq 7$ s ($N = 100$) – Table 2) as also confirmed in the whole numerical assessment (Table 2).

Similar conclusions hold true when wider apertures are at hand as for the example with $N = 900$ elements [$N^{(0)} = N^{(1)} = 30$ – $\boldsymbol{a}^{(p)}$ ($p = 0,\ 1$) → (30, 15, 7, 22)-ADS], whose PSL behaviour and optimal radiation patterns are provided in Figs. 4*b* and *d*, respectively. In this latter case, the efficiency of the synthesis process is further pointed out by the fact that the PSL^{opt} of the optimal design (Fig. 4*d*) turns out to be quite close to that of the single-beam $N = 900$ fully populated uniform arrangement (PSL$\simeq -13.5$ dB). Moreover, the average sidelobe level ranges in a smaller interval (i.e. $-11.1 \le \text{PSL}^{\text{ave}} \le -7.5$ – Fig. 4*b*) than that of the previous test case [$-7.2 \le \text{PSL}^{\text{ave}} \le -5$ dB – Fig. 4*a*].

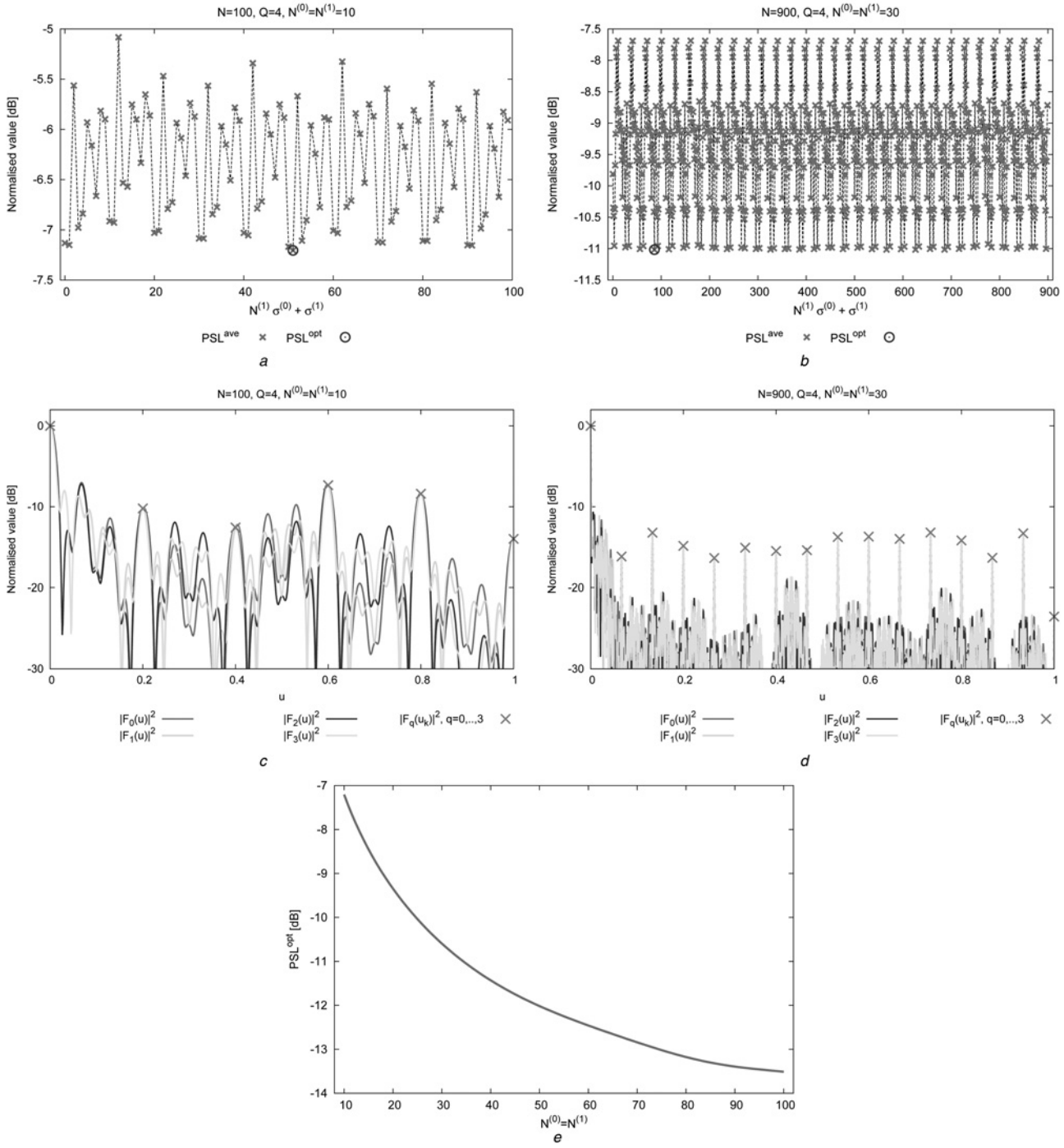

Fig. 4 *Performance analysis ($Q = 4$, $P = 2$, $d = 0.5$, $\nu_q^{(p)} = 0.5$, $N^{(0)} = N^{(P-1)}$) – plots of (a), (b) PSL^{ave} against $\sigma^{(p)}$ ($p = 0$, 1) (c), (d) $F_q(u)$, $q = 0, \ldots, Q - 1$ when*

a and *c* $N^{(0)} = 10$
b and *d* $N^{(0)} = 30$
e Behaviour of PSL^{opt} against $N^{(0)}$

Table 2 Performance analysis ($Q = 4$) – descriptive parameters and PSL performance

Test cases	N	$\boldsymbol{a}^{(0)}$	$\boldsymbol{a}^{(1)}$	$\sigma_{opt}^{(0)}$	$\sigma_{opt}^{(1)}$	Δt, s	PSL^{opt}, dB	D^{opt}, dB	BW^{opt}, deg
Fig. 4*c*	100	(10, 5, 2, 7)	(10, 5, 2, 7)	5	1	7.03	−7.02	13.9	1.26
Fig. 4*d*	900	(30, 15, 7, 22)	(30, 15, 7, 22)	2	26	1.82×10^{1}	−11.01	23.5	1.16×10^{-1}
Fig. 5*b*	1560	(52, 26, 12, 13)	(30, 15, 7, 22)	21	26	1.44×10^{2}	−11.02	25.9	6.72×10^{-2}
Fig. 5*c*	5200	(52, 26, 12, 13)	(100, 50, 24, 25)	51	10	2.79×10^{2}	−12.74	31.1	1.96×10^{-2}
Fig. 6*b*	1560	(30, 15, 7, 22)	(52, 26, 12, 13)	12	14	1.40×10^{2}	−12.59	25.9	6.85×10^{-2}
Fig. 6*c*	5200	(100, 50, 24, 25)	(52, 26, 12, 13)	14	66	2.88×10^{2}	−12.60	31.1	2.05×10^{-2}
Fig. 7	2809	(53, 14, 3, 26)	(53, 14, 3, 26)	39	14	1.20×10^{2}	−9.04	27.3	3.61×10^{-2}

doi: 10.1049/iet-map.2013.0697

This suggests that increasing the sequence length can result in lower sidelobes of the interleaved arrangements despite the increased complexity of the synthesis problem.

To investigate such an issue, the value of PSL^{opt} has been computed in correspondence with different linear distributions characterised by $N^{(0)} = N^{(1)} \in [10, 100]$ (Fig. 4*e*). As it can be observed, the peak level decreases with the sequence length until a stationary value Fig. 4*e* close to that of the uniform arrangement (i.e. −13.5 dB) as predicted by the 'ADS' theory [22]. Such a behaviour is related to the isophoric nature of the considered problem (see 'fully interleaving problem'). Nevertheless, lower sidelobes could be obtained by applying suitable amplitude tapering to the 'ADS' layouts (i.e. through hybrid design approaches [33]).

Moreover, as concerns the behaviour of D^{opt} and BW^{opt}, the values reported in Table 2 show that larger apertures always yield narrower beams (e.g. $BW^{opt}|_{N=100} = 1.26°$

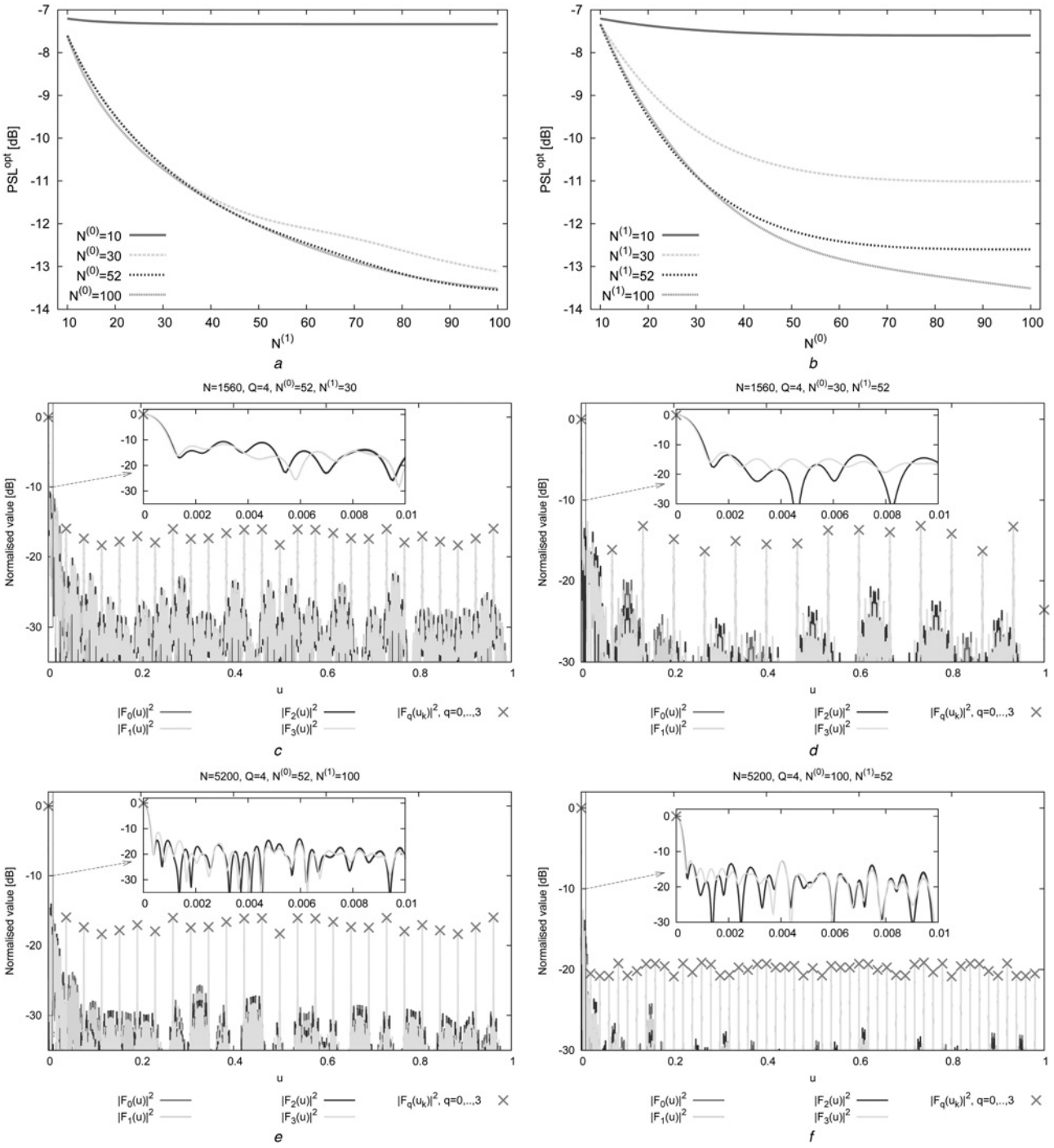

Fig. 5 *Performance analysis ($Q = 4$, $P = 2$, $d = 0.5$, $\nu_q^{(p)} = 0.5$) – plots of PSL^{opt}*

a Against $N^{(P-1)}$ when $N^{(0)} \in \{10, 30, 52, 100\}$
b Against $N^{(0)}$ when $N^{(P-1)} \in 10, 30, 52, 100\}$, and behaviour of $F_q(u)$, $q = 0, \ldots, Q - 1$
c $N^{(0)} = 52 - N^{(P-1)} = 30$
d $N^{(0)} = 30 - N^{(P-1)} = 52$
e $N^{(0)} = 52 - N^{(P-1)} = 100$
f $N^{(0)} = 100 - N^{(P-1)} = 52$

against $BW^{opt}|_{N=900} = 1.16 \times 10^{-1}$°) with higher directivities (e.g. $D^{opt}|_{N=100} = 13.9$ dB against $D^{opt}|_{N=900} = 23.5$ dB), as expected. More in detail, the directivity does not depend on q because of the balanced nature of the arrangements (i.e. $D\{\boldsymbol{w}_q\}|_{N=900} = D^{opt}|_{N=900} = 23.5$ dB $\forall q \in 0, \ldots, 3$ – Fig. 4*d*). Furthermore, small BW variations are observed (e.g. $BW\{\boldsymbol{w}_q\}|_{N=100} \in [1.18, 1.35]$ ° – Fig. 4*d*), especially for wider apertures (e.g. $BW\{\boldsymbol{w}_q\}|_{N=900} \in [1.14 \times 10^{-1}, 1.18 \times 10^{-1}]$° – Fig. 4*d*). Such a result suggests that balanced arrangements yield very similar figures of merit for the Q interleaved functions.

In previous examples, the condition $N^{(0)} = N^{(1)}$ has been imposed, however, different-size aggregations (i.e. $N^{(0)} \neq N^{(1)}$) are of interest when the 'field-of-view' (The beamwidth of $F_q^{(0)}(u)$, $q = 0,\ldots Q-1$.) has to be fine tuned [28]. Accordingly, next examples consider a set of fixed $N^{(0)}$ values ($N^{(0)} = \{10, 30, 52, 100\}$) and vary $N^{(1)}$ in the range [10, 100] [the values of the synthesised PSL are reported in (Fig. 5*a*)]. Similarly, the case $N^{(0)} = N^{(1)}$, the value of PSL^{opt} monotonically decreases with $N^{(1)}$ whatever $N^{(0)}$ (Fig. 5*a*), except for very small $N^{(0)}$ values (e.g. $N^{(0)} = 10$) (Fig. 5*a*). Asymptotically, an arrangement with $N^{(0)} = 30$ is already sufficient to reach the limit of -13.5 dB (Fig. 5*a*), whereas larger $N^{(0)}$ do not significantly contribute to the peak sidelobe reduction (Fig. 5*a*).

By analysing the plots of the optimal beams obtained when $N^{(0)} = 52$ ($N^{(1)} = \{30, 100\}$ – Figs. 5*c* and *e*), one can note that the sidelobes far from the mainbeam turn out to be well below the -13.5 dB limit as expected from 'ADS' properties [22]. Indeed, the peak sidelobes are concentrated around the mainbeam (Fig. 5*a* and *c*) when large arrays are at hand, whereas the radiation to/from the remaining angular directions is less and less significant as $N^{(1)}$ increases (Fig. 5*c* against *e*). Asymptotically, the pattern content outside the mainlobe regions is limited to the a-priori known pattern samples (13) (i.e. the crosses in Fig. 5*e*).

The peak sidelobe reduction until the limit value also verifies when $N^{(1)}$ is kept fixed ($N^{(1)} = \{10, 30, 52, 100\}$) while varying $N^{(0)}$ (the behaviour of PSL^{opt} against $N^{(1)}$ is reported in Fig. 5*b*). Similar conclusions as those from the previous analysis can be yielded, as well, but here the 'PSL' improvement depends on $N^{(1)}$. Consequently, it can be inferred from Figs. 5*a* and *b* that PSL^{opt} mainly depends on

$$N^{\min} \triangleq \min_{p=0,\ldots,P-1} \left\{ N^{(p)} \right\}$$

while the total sequence size N only affects it to a minor extent.

As for the optimal layouts synthesised when $N^{(0)} = \{30, 100\}$ (as a representative example, the radiation patterns obtained when $N^{(1)} = 52$ are reported in Figs. 5*d* and *f*), it turns out that the effect of $N^{(0)}$ on the 'far sidelobes' is much more important than that of $N^{(1)}$ whose variation does not affect the predicted pattern samples. Indeed, it turns out that the average value of these latter is almost constant when changing $N^{(1)}$ from 30 to 100, being $N^{(0)} = 52$ [$(N^{(0)} = 52, N^{(1)} = 30)$: $\left[1/\{N^{(0)} - 1\}\right] \sum_{k=1}^{N^{(0)}-1} \left| F_q\left([k/(d^{(0)}N^{(0)})]\right)\right| = -17.07$ dB – Fig. 5*c*; $(N^{(0)} = 52, N^{(1)} = 100)$: $\left[1/\{N^{(0)} - 1\}\right] \sum_{k=1}^{N^{(0)}-1} \left| F_q\left(k/\{d^{(0)}N^{(0)}\}\right)\right| = -17.07$ dB – Fig. 5*e*], while there is a non-negligible variation for the complementary case $[(N^{(0)} = 30, N^{(1)} = 52)$: $\left[1/\{N^{(0)} - 1\}\right] \sum_{k=1}^{N^{(0)}-1} \left| F_q\left(k/\{d^{(0)}N^{(0)}\}\right)\right| = -14.62$ dB – Fig. 5*d*; $(N^{(0)} = 100, N^{(1)} = 52)$: $\left[1/\{N^{(0)} - 1\}\right] \sum_{k=1}^{N^{(0)}-1} \left| F_q\left([k/\{d^{(0)}N^{(0)}\}]\right)\right| = -19.95$ dB – Fig. 5*f*]. This is actually motivated by (6), since the envelope of F_q is determined by the pattern component of the subarray $N^{(0)}$ in size, $F_q^{(0)}$.

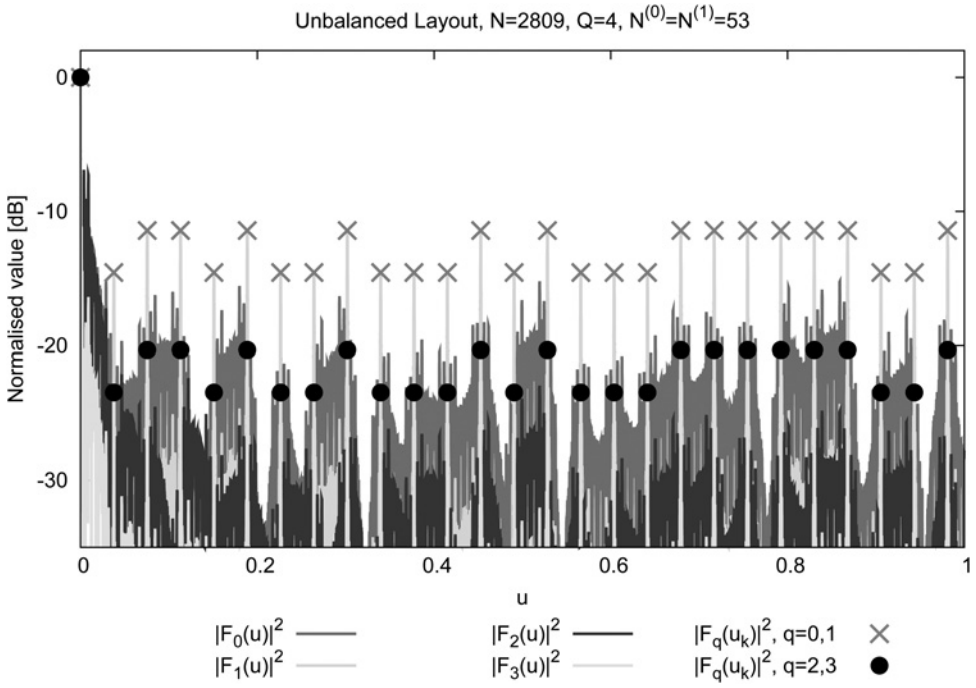

Fig. 6 *Performance analysis ($Q = 4$, $P = 2$, $d = 0.5$, $N^{(0)} = N^{(P-1)} = 53$) – plot of $F_q(u)$ along with the predictable pattern samples $\left|F_q\left([k/\{d^{(0)}N^{(0)}\}]\right)\right|^2$, $q = 0, \ldots, Q-1$*

doi: 10.1049/iet-map.2013.0697

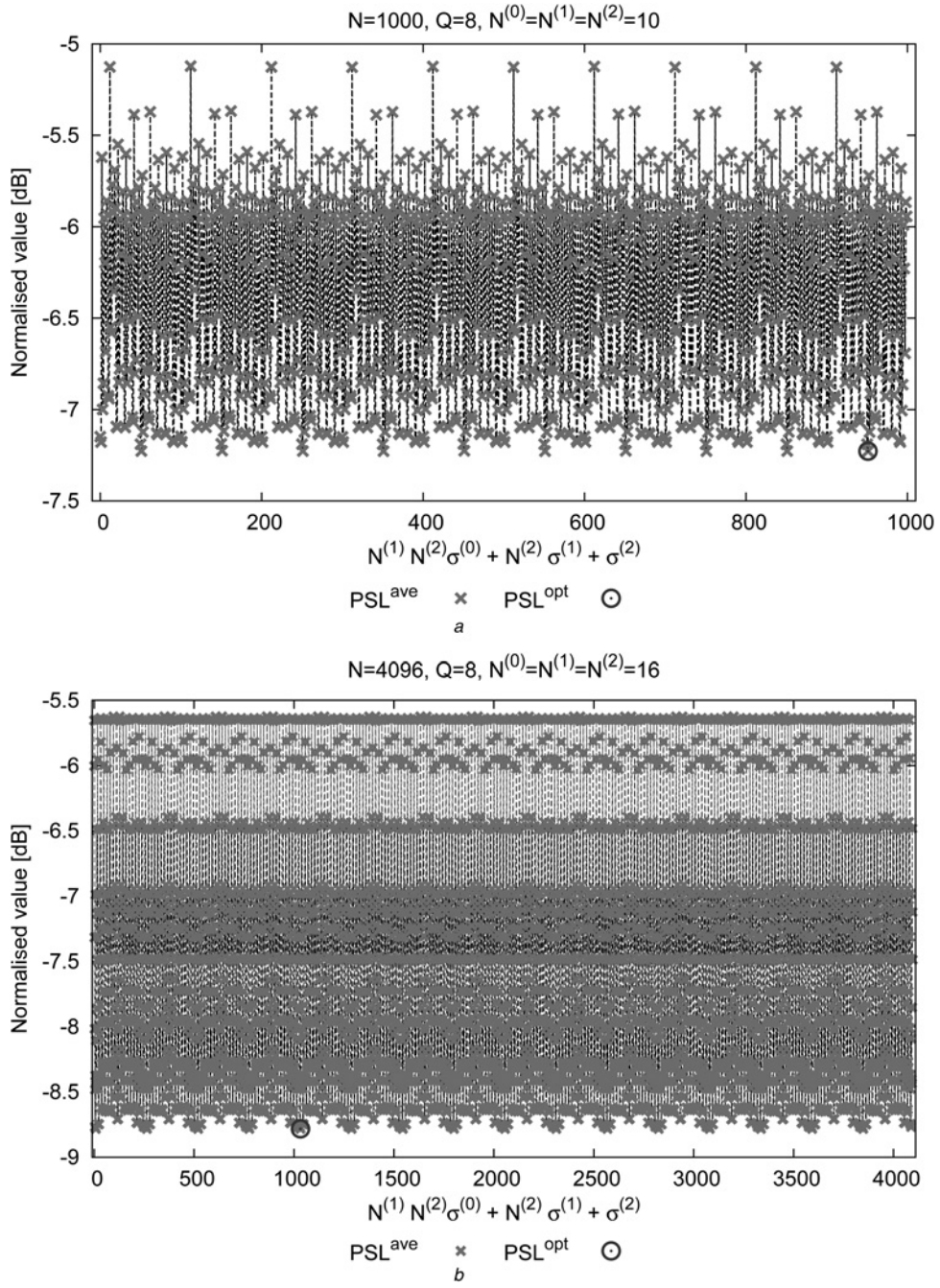

Fig. 7 *Performance analysis ($Q = 8$, $P = 3$, $d = 0.5$, $v_q^{(p)} = 0.5$, $N^{(0)} = N^{(1)} = N^{(P-1)}$) – plots of PSL^{ave} and PSL^{opt} against $\sigma^{(p)}$ ($p = 0, \ldots, P - 1$)*

a $N^{(0)} = N^{(1)} = N^{(P-1)} = 10$

b $N^{(0)} = N^{(1)} = N^{(P-1)} = 16$

Whether well-controlled sidelobes can be obtained dealing with 'balanced' layouts (i.e. $v_q^{(p)} = 0.5$, $q \in [0, Q - 1]$, $p \in [0, P - 1]$), the same still holds true when unbalanced 'ADS' arrangements are used. To provide a deeper insight on this, the next numerical experiment is concerned with a lattice of $N = 2809$ elements partitioned into $N^{(0)} = N^{(1)} = 53$ unbalanced ADS[(53, 14, 3, 26)] to yield $Q = 4$ beams with different radiation features.

The plots of the optimal patterns in Fig. 6 indicate that no grating lobes appear whatever $q = 0, \ldots, Q - 1$, whereas the predictable pattern samples differ $\left(\left|F_r\left(\left[k/\left\{d^{(p)}N^{(p)}\right\}\right]\right)\right|^2 \neq \left|F_s\left(\left[k/\left\{d^{(p)}N^{(p)}\right\}\right]\right)\right|^2\right)$ for an a-priori known offset since their pth components differ $\left(\left|F_r^{(p)}\left(\left[k/\left\{d^{(p)}N^{(p)}\right\}\right]\right)\right|^2 \neq \left|F_s^{(p)}\left(\left[k/\left\{d^{(p)}N^{(p)}\right\}\right]\right)\right|^2\right.$, $r \neq s$ ($r, s \in [0, Q - 1]$) being $\left(N^{(p)} - 2K_0^{(p)}\right) \neq 0$ ($p = 0, 1$) in (13). Those controllable differences can be profitably exploited to generate different radiation performances on the same physical aperture.

4.2 Shared aperture arrays with $Q > 4$ interleaved functions

To assess the reliability and the flexibility of the proposed approach, a higher complexity problem is addressed in the

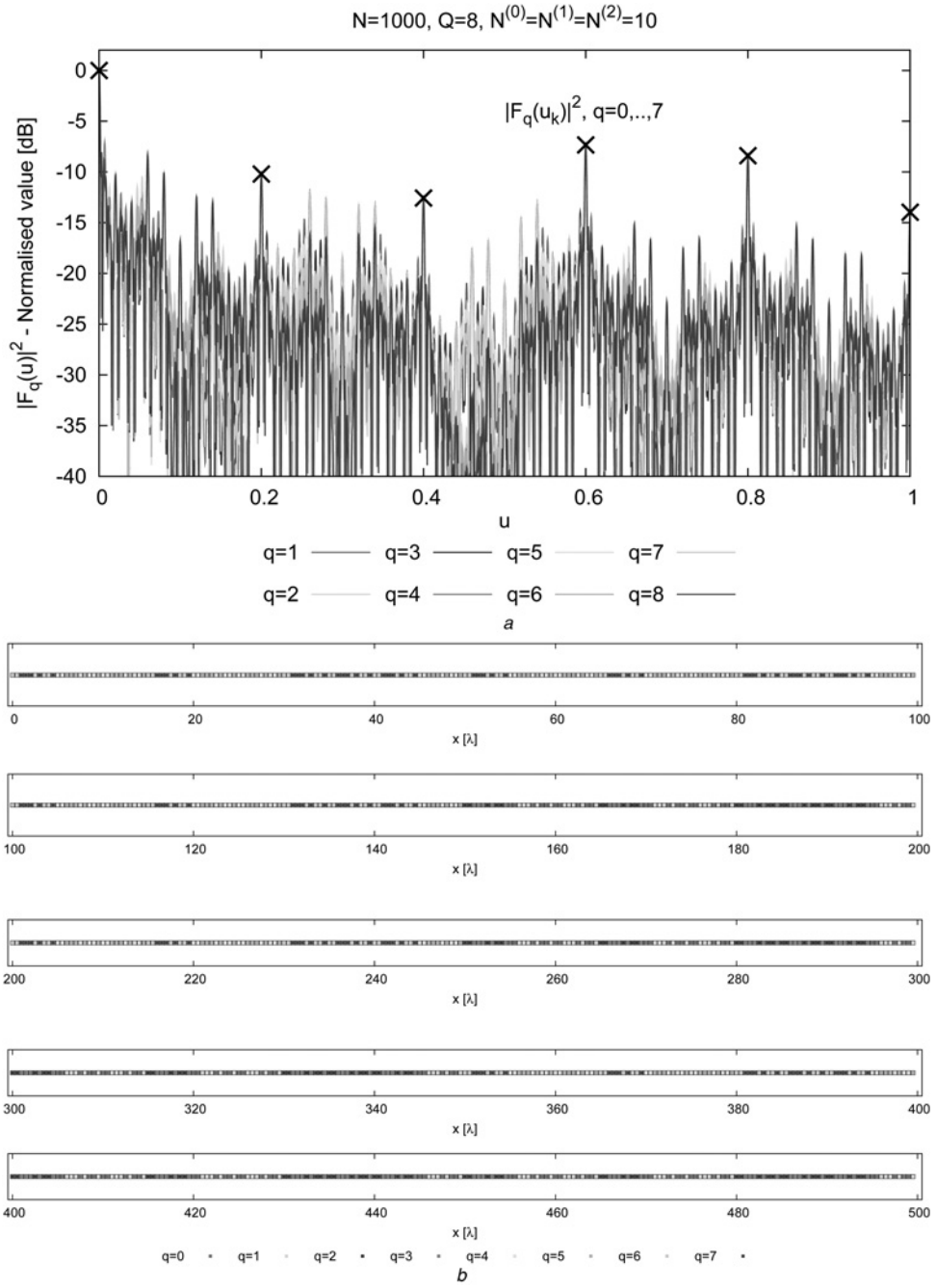

Fig. 8 *Performance analysis ($Q = 8$, $P = 3$, $d = 0.5$, $v_q^{(p)} = 0.5$, $N^{(0)} = N^{(1)} = N^{(P-1)} = 10$) – plots of*

a $F_q(u)$, $q = 0, \ldots, Q - 1$

b Associated interleaved arrangements

final example concerned with a $Q = 8$ ($P = 3$) interleaved array. With reference to a regular lattice of $N = 1000$ elements spaced by $d = 0.5$, the (10, 5, 2, 7)-ADS has been used to define $\boldsymbol{s}_0^{(p)}$ under the assumption that $N^{(0)} = N^{(1)} = N^{(2)} = 10$.

The plot of $\mathrm{PSL}^{\mathrm{ave}}$ against the cyclic shift index in Fig. 7*a* shows that despite the average spacing of $d_q = 4$ and the low number of elements associated to each qth function ($K_q = 125$, $q = 0, \ldots, 7$ – 'ADS' architecture reported in Fig. 8*b*), the grating lobes are avoided also in this case (i.e. $\mathrm{PSL}^{\mathrm{ave}} \neq 0$ dB $\rightarrow -7.3 \leq \mathrm{PSL}^{\mathrm{ave}} \leq -5.1$ dB – Fig. 7*a*). Moreover, the optimal layout (Fig. 8*b*) has a peak sidelobe ($\mathrm{PSL}^{\mathrm{opt}} = -7.22$ dB – Fig. 8*a*) comparable with that of the $Q = 2$ array with $N^{(0)} = N^{(1)} = 10$ (Fig. 4*c* – $\mathrm{PSL}^{\mathrm{opt}} = -7.02$ dB). Such an observation further assesses the conclusion that the average 'PSL' of the ADS-interleaved array mainly depends on the parameters $N^{(p)}$, $p = 0, \ldots, P - 1$ rather than by the number of interleaved functions, Q. This is also confirmed for larger layouts as it is shown in Fig. 7*b* where the $\mathrm{PSL}^{\mathrm{ave}}$ values of an $N = 4096$ array with $Q = 8$ functions are reported. Indeed, as expected, both $\mathrm{PSL}^{\mathrm{opt}}$ and the average value of $\mathrm{PSL}^{\mathrm{ave}}$ reduce with respect to the $N = 1000$ case (Figs. 7*a* against *b*): $\mathrm{PSL}^{\mathrm{opt}}\rfloor_{N=4096} = -8.87$ dB against $\mathrm{PSL}^{\mathrm{opt}}\rfloor_{N=1000} = -7.22$ dB; $(1/N)\sum_{\sigma_0=0}^{N^{(0)}-1}\sum_{\sigma_1=0}^{N^{(1)}-1}\mathrm{PSL}^{\mathrm{ave}}\rfloor_{N=4096} = -7.75$ dB against $(1/N)\sum_{\sigma_0=0}^{N^{(0)}-1}\sum_{\sigma_1=0}^{N^{(1)}-1}\mathrm{PSL}^{\mathrm{ave}}\rfloor_{N=1000} = -6.38$ dB.

doi: 10.1049/iet-map.2013.0697

5 Conclusions and remarks

An innovative approach for the analytical design of fully interleaved arrays supporting more functionalities on the same shared aperture has been proposed in this paper, which is not aimed at finding an optimal interleaving scheme for a specific design problem, but rather at giving simple and reliable guidelines for the design of non-overlapped layouts exhibiting low and predictable 'PSL' values. Towards this end, a hierarchical ADS-based methodology has been introduced. By means of a subarraying strategy that exploits $P = \log_2 Q$ suitable 'ADS' sequences, the proposed approach proved to be able to interweave Q independent functions with a-priori known beam features.

The obtained results have pointed out the following features of the 'ADS' hierarchical interleaving scheme:

- An arbitrary number of independent functions can be fully interleaved by suitably selecting the number of hierarchical levels P (Section 3).
- The design procedure is computationally efficient also for large apertures and Q values since it just requires a simple shifting of reference 'ADS' sequences widely available in open-access repositories [31] (Section 3.3).
- Thanks to the 'ADS' autocorrelation features, the approach avoids the occurrence of grating lobes in any qth independent beam and predictable pattern samples are available whatever Q (Section 4).
- The approach is suitable for synthesising both balanced and unbalanced architectures, thus per-function 'PSL' constraints can be effectively taken into account (Section 4.1).
- Owing to their isophoric and non-overlapped nature, sidelobe values in the range $\mathrm{PSL}^{\mathrm{opt}} \in [-7.02\ \mathrm{dB},\ -12.74\ \mathrm{dB}]$ are obtained (Table 2), thus making unlikely their direct application (i.e. without tapering) in 'PSL' demanding systems; however, ADS-based layouts can be profitably used as initial trial solutions for enhancing the convergence rate of multiple-agent evolutionary algorithms towards optimal-PSL architectures as already proved in other array synthesis problems [26, 27].

In addition to these features, other main contributions of this paper consist in the following methodological novelties:

1. An extended formulation for the analysis of subarray-based architectures comprising an arbitrary number of aggregation levels P [(5)–(7)] that generalises the subarray pattern multiplication formula [7] (Section 3.1).
2. A generalised 'ADS' interleaving approach that extends the method in [17] (Section 3.3).

Future works will be aimed, on the one hand, at extending the proposed design approach to other array geometries and, on the other hand, at taking into account in the mathematical derivation the mutual coupling effects among the array elements as well as the possible tolerances to other parameter variations (i.e. frequency). Moreover, an analysis of the relations among the maximum Q, the physical size of the elements and the lattice spacings in practical multi-band designs will be the subject of future numerical and experimental assessments, along with an investigation of the array phase centre location and its possible shifting in the considered architecture.

6 References

1 Naishadham, K., RongLin, L., Lim, Y., Wu, T., Hunsicker, W., Tentzeris, M.: 'A shared-aperture dual-band planar array with self-similar printed folded dipoles', *IEEE Trans. Antennas Propag.*, 2013, **61**, (2), pp. 606–613
2 Hemmi, C., Dover, R.T., German, F., Vespa, A.: 'Multifunction wideband array design', *IEEE Trans. Antennas Propag.*, 1999, **47**, pp. 425–431
3 Coman, C.I., Lager, I.E., Ligthart, L.P.: 'The design of shared aperture antennas consisting of differently sized elements', *IEEE Trans. Antennas Propag.*, 2006, **54**, (2), pp. 376–383
4 Pozar, D.M., Targonski, S.D.: 'A shared-aperture dual-band dualpolarized microstrip array', *IEEE Trans. Antennas Propag.*, 2001, **49**, pp. 150–157
5 Zhong, S.-S., Sun, Z., Kong, L.-B., Gao, C., Wang, W., Jin, M.-P.: 'Tri-band dual-polarization shared-aperture microstrip array for SAR applications', *IEEE Trans. Antennas Propag.*, 2012, **60**, (9), pp. 4157–4165
6 Haupt, R.L.: 'Interleaved thinned linear arrays', *IEEE Trans. Antennas Propag.*, 2005, **53**, (9), pp. 2858–2864
7 Haupt, R.L.: 'Antenna arrays – a computational approach' (Wiley, Hoboken, NJ, 2010)
8 Oliveri, G., Rocca, P., Massa, A.: 'Interleaved linear arrays with difference sets', *Electron. Lett.*, 2010, **46**, (5), pp. 323–324
9 Lager, I.E., Trampuz, C., Simeoni, M., Ligthart, L.P.: 'Interleaved array antennas for FMCW radar applications', *IEEE Trans. Antennas Propag.*, 2009, **57**, (8), pp. 2486–2490
10 Hsiao, J.: 'Analysis of interleaved arrays of waveguide elements', *IEEE Trans. Antennas Propag.*, 1971, **19**, pp. 729–735
11 Simeoni, M., Lager, I.E., Coman, C.I., Roederer, A.G.: 'Implementation of polarization agility in planar phased-array antennas by means of interleaved sub-arrays', *Radio Sci.*, 2009, **44**, RS5013, pp. 1–12
12 Boyns, J., Provencher, J.: 'Experimental results of a multifrequency array antenna', *IEEE Trans. Antennas Propag.*, 1972, **20**, pp. 106–107
13 Stangel, J., Punturieri, J.: 'Random subarray techniques in electronic scan antenna design'. Proc. IEEE AP-S Symp., December 1972, pp. 17–20
14 Haupt, R.L., Werner, D.H.: 'Genetic algorithms in electromagnetics' (Wiley, Hoboken, NJ, 2007)
15 D'Urso, M., Isernia, T.: 'Solving some array synthesis problems by means of an effective hybrid approach', *IEEE Trans. Antennas Propag.*, 2007, **55**, (3), pp. 750–759
16 Ahmad, A., Behera, A.K., Mandal, S.K., Mahanti, G.K., Ghatak, R.: 'Artificial bee colony algorithm to reduce the side lobe level of uniformly excited linear antenna arrays through optimized element spacing'. Proc. IEEE Conf. Information and Communication Tech., Jeju, Island, 11–12 April 2013, pp. 1029–1032
17 Oliveri, G., Massa, A.: 'Fully-interleaved linear arrays with predictable sidelobes based on almost difference sets', *IET Radar Sonar Navig.*, 2010, **4**, (5), pp. 649–661
18 Oliveri, G., Massa, A.: 'ADS-based array design for 2D and 3D ultrasound imaging', *IEEE Trans. Ultrason. Ferroelectr. Freq. Control*, 2010, **57**, (7), pp. 1568–1582
19 Oliveri, G., Donelli, M., Massa, A.: 'Genetically-designed arbitrary length almost difference sets', *Electron. Lett.*, 2009, **45**, (23), pp. 1182–1183
20 Arasu, K.T., Ding, C., Helleseth, T., Kumar, P.V., Martinsen, H.M.: 'Almost difference sets and their sequences with optimal autocorrelation', *IEEE Trans. Inf. Theory*, 2001, **47**, (7), pp. 2934–2943
21 Leeper, D.G.: 'Isophoric arrays – massively thinned phased arrays with well-controlled sidelobes', *IEEE Trans. Antennas Propag.*, 1999, **47**, (12), pp. 1825–1835
22 Oliveri, G., Donelli, M., Massa, A.: 'Linear array thinning exploiting almost difference sets', *IEEE Trans. Antennas Propag.*, 2009, **57**, (12), pp. 3800–3812
23 Oliveri, G., Manica, L., Massa, A.: 'On the impact of mutual coupling effects on the PSL performances of ADS thinned arrays', *Prog. Electromagn. Res. B*, 2009, **17**, pp. 293–308
24 Oliveri, G., Manica, L., Massa, A.: 'ADS-based guidelines for thinned planar arrays', *IEEE Trans. Antennas Propag.*, 2010, **58**, (6), pp. 1935–1948
25 Oliveri, G., Caramanica, F., Fontanari, C., Massa, A.: 'Rectangular thinned arrays based on McFarland difference sets', *IEEE Trans. Antennas Propag.*, 2011, **59**, (5), pp. 1546–1552
26 Oliveri, G., Caramanica, F., Massa, A.: 'Hybrid ADS-based techniques for radio astronomy array design', *IEEE Trans. Antennas Propag.*, 2011, **59**, (6), pp. 1817–1827

27 Oliveri, G., Massa, A.: 'Genetic algorithm (GA)-enhanced almost difference set (ADS)-based approach for array thinning', *IET Microw. Antennas Propag.*, 2011, **5**, (3), pp. 305–315

28 Mailloux, R.J.: 'Phased array antenna handbook' (Artech House, Inc., Norwood, MA, 2005)

29 Ding, C., Helleseth, T., Lam, K.Y.: 'Several classes of binary sequences with three-level autocorrelation', *IEEE Trans. Inf. Theory*, 1999, **45**, (7), pp. 2606–2612

30 Zhang, Y., Lei, J.G., Zhang, S.P.: 'A new family of almost difference sets and some necessary conditions', *IEEE Trans. Inf. Theory*, 2006, **52**, (5), pp. 2052–2061

31 ELEDIA Almost Difference Set Repository. Available at http://www.eledia.ing.unitn.it/

32 Massa, A., Oliveri, G., Viani, F., Rocca, P.: 'Array designs for long-distance wireless power transmission: state-of-the-art and innovative solutions', *Proc. IEEE*, 2013, **101**, (6), pp. 1464–1481

33 Sartori, D., Oliveri, G., Manica, L., Massa, A.: 'Hybrid design of non-regular linear arrays with arbitrary upper bounds on the far-field power pattern', *IEEE Trans. Antennas Propag.*, 2013, **61**, (12), pp. 6237–6242

7 Appendix

7.1 Proof of (4)

To prove that $w_q(n)$ in Fig. 1 complies with (4), let us apply the induction principle. More in detail, the aim is to verify that (*a*) (4) holds true when $P=1$ and (*b*) if (4) holds when $P=\widetilde{P}$, then the same verifies when $P=\widetilde{P}+1$.

As for the logical step (*a*), (4) when $P=1$ case (i.e. the case of single-level interleaving) reduces to

$$w_q(n)\Big|_{P=0} = s_q^{(0)}\left(n\rfloor_{\mathrm{mod}N^{(0)}}\right) = s_q^{(0)}(n)$$
$$n=0,\ \ldots,\ N^{(0)}-1$$

and the effective weights turn out to be equivalent to those of the 0th sequence alone.

Concerning (*b*), let us now assume that (4) holds true for a given $P=\widetilde{P}$. It is then possible to write that

$$w_q(n)\Big|_{P=\widetilde{P}} = \prod_{p=0}^{\widetilde{P}-1} s_q^{(p)}\left[\left(n \div L^{(p-1)}\right)\rfloor_{\mathrm{mod}N^{(p)}}\right]$$
$$n=0,\ \ldots,\ L^{(\widetilde{P})}-1$$

where the length of the sequence is expressed as $L^{(\widetilde{P})}=\prod_{p=0}^{\widetilde{P}-1}N^{(p)}$. By observing Fig. 1, it can be inferred that the weights of the case $P=\widetilde{P}+1$ are the replicated and weighted version of those at the $\widetilde{P}$th level

$$w_q(n)\Big|_{P=\widetilde{P}+1} = \begin{cases} w_q(n)\Big|_{P=\widetilde{P}} \times s_q^{(\widetilde{P})}(0) & \text{if } 0 \le n < L^{(\widetilde{P})} \\ w_q(n)\Big|_{P=\widetilde{P}} \times s_q^{(\widetilde{P})}(1) & \text{if } L^{(\widetilde{P})} \le n < 2L^{(\widetilde{P})} \\ \vdots & \vdots \\ w_q(n)\Big|_{P=\widetilde{P}} \times s_q^{(\widetilde{P})}\left(N^{(\widetilde{P})}\right) & \text{if } \left(N^{(\widetilde{P})}-2\right)L^{(\widetilde{P})} \le n < \left(N^{(\widetilde{P})}-1\right)L^{(\widetilde{P})} \end{cases} \tag{18}$$

By means of simple mathematical manipulations, it results that

$$w_q(n)\Big|_{P=\widetilde{P}+1} = w_q(n)\Big|_{P=\widetilde{P}} \times s_q^{(\widetilde{P})}\left[\left(n \div L^{(\widetilde{P})}\right)\rfloor_{\mathrm{mod}N^{(\widetilde{P}+1)}}\right]$$

Such an expression is equivalent to (4) when $P=\widetilde{P}+1$.

7.2 Derivation of (5)

By substituting (4) in (2), it results that the qth beam exhibits the following array factor (see (19))

To simplify such an expression, let us firstly rewrite the term within curly brackets as

$$\begin{aligned} &\prod_{p=0}^{P-1} s_q^{(p)}\left[\left(n \div L^{(p-1)}\right)\rfloor_{\mathrm{mod}N^{(p)}}\right] \\ &= \beta_q^{(P-2)}(n) \times s_q^{(P-1)}\left[\left(n \div L^{(P-2)}\right)\rfloor_{\mathrm{mod}N^{(P-1)}}\right] \end{aligned} \tag{20}$$

where $\beta_q^{(P-2)}(n) \triangleq \left(\prod_{p=0}^{P-2} s_q^{(p)}\left[\left(n \div L^{(p-1)}\right)\rfloor_{\mathrm{mod}N^{(p)}}\right]\right)$. By noting that

$$\begin{aligned} &\left(n \div L^{(P-2)}\right)\rfloor_{\mathrm{mod}N^{(P-1)}} \\ &= \left(n \div L^{(P-2)}\right)\rfloor_{\mathrm{mod}\frac{N^{(P-1)}L^{(P-2)}}{L^{(P-2)}}} \\ &= \left(n \div L^{(P-2)}\right)\rfloor_{\mathrm{mod}\frac{N}{L^{(P-2)}}} = \left(n \div L^{(P-2)}\right) \end{aligned} \tag{21}$$

it turns out that (see (22))

By considering that $\beta_q^{(P-2)}(n)$ is periodic with period $L^{(P-2)}$ (i.e. $\beta_q^{(P-2)}(n)=\beta_q^{(P-2)}\left(n+rL^{(P-2)}\right)$, $r=0,\ldots,N^{(P-1)}-1$),

$$F_q(u) = \frac{\sum_{n=0}^{N-1}\left\{\prod_{p=0}^{P-1} s_q^{(p)}\left[\left(n \div L^{(p-1)}\right)\rfloor_{\mathrm{mod}N^{(p)}}\right]\right\}\exp(i2\pi n\,\mathrm{d}u)}{\prod_{p=0}^{P-1}K_q^{(p)}}, \quad q=0,\ \ldots,\ Q-1 \tag{19}$$

$$F_q(u) = \frac{\sum_{n=0}^{N-1}\left\{\beta_q^{(P-2)}(n) \times s_q^{(P-1)}\left(n \div L^{(P-2)}\right)\right\}\exp(i2\pi n\,\mathrm{d}u)}{\prod_{p=0}^{P-1}K_q^{(p)}}, \quad q=0,\ \ldots,\ Q-1 \tag{22}$$

doi: 10.1049/iet-map.2013.0697

(19) can be rewritten as follows

$$F_q(u) = \frac{1}{\prod_{p=0}^{P-1} K_q^{(p)}} \sum_{r=0}^{N^{(P-1)}-1} \sum_{n=0}^{L^{(P-2)}-1} \left\{ \beta_q^{(P-2)}(n) \times s_q^{(P-1)}(r) \exp\left[i2\pi \left(n + rL^{(P-2)} \right) \mathrm{d}u \right] \right\}$$

which, by simple manipulations, is equal to

$$F_q(u) = \left[\frac{\sum_{n=0}^{N^{(P-2)}-1} \left\{ \beta_q^{(P-2)}(n) \right\} \exp(i2\pi n \, \mathrm{d}u)}{\prod_{p=0}^{P-2} K_q^{(p)}} \right] \times \left[\frac{\sum_{r=0}^{N^{(P-1)}-1} \left\{ s_q^{(P-1)}(r) \exp\left[i2\pi r L^{(P-2)} \, \mathrm{d}u \right] \right\}}{K_q^{(P-1)}} \right] = \left[\frac{\sum_{n=0}^{N^{(P-2)}-1} \left\{ \beta_q^{(P-2)}(n) \right\} \exp(i2\pi n \, \mathrm{d}u)}{\prod_{p=0}^{P-2} K_q^{(p)}} \right] \times F_q^{(P-1)}(u) \tag{23}$$

By iteratively applying the same procedure to the term within square brackets in (26), it finally results that

$$F_q(u) = F_q^{(P-1)}(u) \times F_q^{(P-2)}(u) \times \cdots \times F_q^{(0)}(u) \quad q = 0, \ \ldots, \ Q-1$$

7.3 Derivation of (11)

According to (10), the number of 'active' elements generating the qth function is equal to

$$\sum_{q=0}^{Q-1} K_q = N \sum_{q=0}^{Q-1} \left[\left(\prod_{p=0}^{P-1} \nu_q^{(p)} \right) \right] \tag{24}$$

where

$$\nu_q^{(p)} = \frac{1}{N^{(p)}} \left(\sum_{n=0}^{N^{(p)}} s_q^{(p)}(n) \right) = \begin{cases} \dfrac{\left[\sum_{n=0}^{N^{(p)}} \left(1 - s_0^{(p)}(n) \right) \right]}{N^{(p)}} & \text{if } \alpha_q^{(p)} = 1 \\ \dfrac{\left[\sum_{n=0}^{N^{(p)}} \left(s_0^{(p)}(n) \right) \right]}{N^{(p)}} & \text{otherwise} \end{cases} = \begin{cases} \dfrac{\left[N^{(p)} \left(1 - \nu_0^{(p)} \right) \right]}{N^{(p)}} & \text{if } \alpha_q^{(p)} = 1 \\ \dfrac{\left[N^{(p)} \left(\nu_0^{(p)} \right) \right]}{N^{(p)}} & \text{otherwise} \end{cases} = \begin{cases} 1 - \nu_0^{(p)} & \text{if } \alpha_q^{(p)} = 1 \\ \nu_0^{(p)} & \text{otherwise} \end{cases} \tag{25}$$

according to (9). By substituting (25) in (24) and noting that $\alpha_q^{(P-1)} = 0$ if $0 \le q \le (Q/2) - 1$ and $\alpha_q^{(P-1)} = 1$ if $(Q/2) \le q \le Q - 1$, it turns out that

$$\begin{aligned} \sum_{q=0}^{Q-1} K_q &= N \left\{ \sum_{q=0}^{Q-1} \left[\left(\prod_{p=0}^{P-1} \nu_q^{(p)} \right) \right] \right\} \\ &= N \left\{ \sum_{q=0}^{Q-1} \left[\left(\prod_{p=0}^{P-2} \nu_q^{(p)} \right) \times \nu_q^{(P-1)} \right] \right\} \\ &= N \left\{ \sum_{q=0}^{\frac{Q}{2}-1} \left[\nu_0^{(P-1)} \times \left(\prod_{p=0}^{P-2} \nu_q^{(p)} \right) \right] + \sum_{q=Q/2}^{Q-1} \left[\left(1 - \nu_0^{(P-1)} \right) \times \left(\prod \prod_{p=0}^{P-2} \nu_q^{(p)} \right) \right] \right\} \\ &= N \left\{ \nu_0^{(P-1)} \times \sum_{q=0}^{\frac{Q}{2}-1} \left[\left(\prod_{p=0}^{P-2} \nu_q^{(p)} \right) \right] + \left(1 - \nu_0^{(P-1)} \right) \times \sum_{q=Q/2}^{Q-1} \left[\left(\prod_{p=0}^{P-2} \nu_q^{(p)} \right) \right] \right\} \end{aligned} \tag{26}$$

By observing that $\sum_{q=0}^{\frac{Q}{2}-1} \left[\left(\prod_{p=0}^{P-2} \nu_q^{(p)} \right) \right] = \sum_{q=Q/2}^{Q-1} \left[\left(\prod_{p=0}^{P-2} \nu_q^{(p)} \right) \right]$ because of the symmetry of the structure under analysis, the previous relationship can be rewritten as follows

$$\sum_{q=0}^{Q-1} K_q = N \left\{ \sum_{q=0}^{\frac{Q}{2}-1} \left[\left(\prod_{p=0}^{P-2} \nu_q^{(p)} \right) \right] \right\}$$

By iterating $P-1$ times such a simple procedure, one obtains that

$$\sum_{q=0}^{Q-1} K_q = N \left\{ \nu_0^{(0)} + \nu_1^{(0)} \right\}$$

Let us finally note that $\nu_1^{(0)} = \left(1 - \nu_0^{(0)} \right)$ [$\alpha_1^{(0)} = 1$, (25)]. Consequently, (11) is yielded.

7.4 ADS design procedure

According to the derivation in Section 3, the following 'ADS' hierarchical design procedure is deduced:

1. *Input:* Define the number of desired interleaved functions Q and the lattice size N.
2. *ADS selection:* Compute $P = \log_2 Q$, factorise $N = \prod_{p=0}^{P-1} N^{(p)}$, and choose a set of ($N^{(p)}$, $K^{(p)}$, $\Lambda^{(p)}$, $t^{(p)}$) – 'ADS' sequences $\boldsymbol{a}^{(p)}$ ($p = 0, \ldots, P-1$).
3. *Initialisation:* Set $\sigma^{(p)} = 0$ ($p = 0, \ldots, P-1$) and $\mathrm{PSL}^{\mathrm{ave}} = \mathrm{PSL}^{\mathrm{opt}} = 1$.
4. *Loop:* For each shift value $\sigma^{(p)} = 0, \ldots, N^{(p)} - 1$, ($p = 0, \ldots, P-1$), perform the following steps:
   (a) *Weight synthesis:* Compute $\boldsymbol{s}_0^{(p)} = \left\{ a^{(p)} \left[\left(n + \sigma^{(p)} \right) \right]_{\mathrm{mod} N^{(p)}} \right\}, \quad n = 0, \ \ldots, \ N^{(p)} - 1$ ($p = 0, \ldots, P-1$) and determine $\boldsymbol{w}_q$ $(q = 0, \ \ldots, \ Q-1)$ by means of (4) and (9).
   (b) *Update optimal layout:* Evaluate $\mathrm{PSL}^{\mathrm{ave}}$ by (1). If $\mathrm{PSL}^{\mathrm{ave}} < \mathrm{PSL}^{\mathrm{opt}}$ then update $\mathrm{PSL}^{\mathrm{opt}} = \mathrm{PSL}^{\mathrm{ave}}$ and set $\sigma_{\mathrm{opt}}^{(p)} = \sigma^{(p)}$ ($p = 0, \ldots, P-1$).

(c) *Convergence check*: If $\sigma^{(p)} = N^{(p)} - 1$, $p = 0, \ldots, P - 1$, then exit the loop, otherwise continue.

5. *Output:* Evaluate $\boldsymbol{s}_0^{(p)} = \left\{a^{(p)}\left[\left(n + \sigma^{(p)}\right)\right]_{\mathrm{mod}N^{(p)}}\right\}$, $n = 0, \ldots, N^{(p)} - 1\}$ $(p = 0, \ldots, P - 1)$ and 'return' the associated $\boldsymbol{w}_q$ $(q = 0, \ldots, Q - 1)$ [by (4) and (9)].

It is worth remarking that, similarly [17], the above procedure requires the 'Loop' to be performed N times. Moreover, the method discussed in [17] actually coincides with the proposed one when $Q = 2$.

IET Microw. Antennas Propag., 2014, Vol. 8, Iss. 10, pp. 794–808
doi: 10.1049/iet-map.2013.0697